Combustion and Flame 213 (2020) 331–342

Contents lists available at ScienceDirect

Combustion and Flame

journal homepage: www.elsevier.com/locate/combustflame

Particle-resolved simulation and modeling of the conversion rate of coal char in chemical looping with oxygen uncoupling

Mingze Su, Xin Tian, Haibo Zhao*

State Key Laboratory of Coal Combustion, School of Energy and Power Engineering, Huazhong University of Science and Technology, Wuhan 430074, China

ARTICLE INFO

Article history:
Received 20 March 2019
Revised 22 November 2019
Accepted 29 November 2019
Available online 19 December 2019

Keywords:
Chemical looping with oxygen uncoupling
Char oxidation
Char gasification
Single particle model
Particle-resolved simulation

ABSTRACT

The high concentration of CO_2 and low concentration of O_2 at relatively low temperatures of 1123-1223 K are typical reactive atmospheres in the fuel reactor of a chemical looping with oxygen uncoupling (CLOU) unit. Char within this environment can be converted via lean-O_2 oxidation and/or rich-CO_2 gasification. Conventional models, which either considered the oxidation only or considered the oxidation and gasification contributions independently by simply adding the two individual conversion rates together, seem arbitrary. Therefore, it is necessary to quantitatively explore the contributions of the oxidation and the gasification reactions as well as their interactions in CLOU conditions through more detailed particle-resolved simulations.

In this work, a single particle model which described a spherical reacting porous particle with its reacting boundary layer was developed to investigate the conversion characteristics of pulverized coal char in lean-O_2 and/or rich-CO_2 conditions (analogous CLOU conditions). The heterogeneous reaction kinetics developed by Tilghman and Mitchell [35] and the simplified GRI-Mech 3.0 gas-phase reaction kinetics were adopted. It was found that the char conversion rate in CLOU conditions could be basically modeled as the sum of the full oxidation consumption rate and the partial gasification consumption rate, *i.e.* $r_{mix}=\varphi_1 r_{gasi}+r_{oxid}$. The interactions between the oxidation and gasification reactions were elaborated in two aspects: on the one side, the oxidation of coal char in CLOU conditions is within the weak zone II burning region, where the oxidation reaction only happens peripherally and is nearly unaffected by the high concentration of CO_2; on the other side, the gasification reaction within the external layer of the coal char particle is inhibited by the oxidation reaction, consequently the gasification reaction only happens inside the coal char particle where O_2 cannot penetrate into. Based on these understandings, a correlation between the coefficient, φ_1, and the effectiveness factor of the oxidation reaction, η, was proposed to describe the overall char conversion rate in CLOU conditions. Through fitting the simulation results under typical CLOU conditions, the quantitative relationship between φ_1 and η was finally attained.

1. Introduction

Chemical looping combustion (CLC) is a novel technology for fossil fuel utilization with inherent CO_2 separation [1–3]. A schematic view of the CLC system is shown in Fig. 1. Similar to the oxygen supply mode of the blood circulation system of human beings, CLC utilizes the circulation of oxygen carrier (OC) to achieve the oxygen transport between reactors, *i.e.*, the fuel reactor (FR) and air reactor (AR). Fuel and air are introduced into the two reactors separately, thus direct contact between fuel and air can be avoided. Theoretically, OCs with high oxygen potential (Me_xO_y) react with fuel, producing CO_2 and H_2O in FR. H_2O can be easily removed by a simple condensation process, thus high-purity CO_2 can be captured from the exhaust gas of FR. The reduced OCs (Me_xO_{y-1}) are then transferred into the AR and re-oxidized by air therein. A loop is finally formed as the regenerated Me_xO_y particles circulate back into the FR. Eventually, the gas-gas separation pattern in conventional CO_2 capture technologies is replaced by much easier gas-solid separation in CLC, where the one-step combustion process is split into two atmosphere-isolated oxidation/reduction sub-processes. In this way, the total exergy loss of the overall combustion and CO_2 capture process can be reduced, and the energy utilization efficiency is thus improved.

In-situ gasification chemical looping combustion (*i*G-CLC) has been proposed as a technical route for the combustion of solid fuels, like coal and biomass [1,2]. Nevertheless, the gasification of solid fuels in *i*G-CLC is usually the rate limiting step, which makes the overall fuel conversion not fast enough. Chemical looping with

* Corresponding author.
E-mail address: hzhao@mail.hust.edu.cn (H. Zhao).

https://doi.org/10.1016/j.combustflame.2019.11.046
0010-2180/

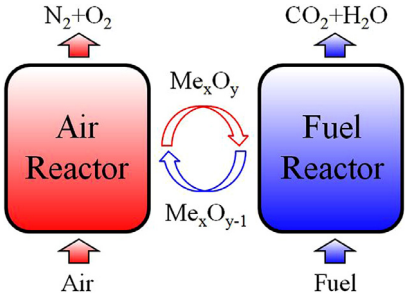

Fig. 1. Schematic view of chemical looping combustion.

oxygen uncoupling (CLOU) was proposed as a high-efficient way for solid fuel combustion [4], which utilizes some special OC materials (such as CuO, Mn_2O_3, Co_3O_4, *etc.*) that are able to release gaseous O_2 at oxygen-deficient atmosphere. Conceptually, these special OCs with high oxygen potential decompose and release gaseous O_2 in FR, thus accelerating the conversion rate of the solid fuels (especially char) greatly [4–6].

In CLOU process, reactions that take place in the FR are very complicated, including, at least, O_2 release from OC decomposition, pyrolysis/oxidation/gasification of solid fuel, heterogeneous reactions between pyrolysis/gasification products and OC, and homogeneous reactions between pyrolysis/gasification products and lean O_2. In order to rationalize the CLOU reactor design and conduct reliable CFD simulation, it is vital to gain insights into the characteristics of the aforementioned reactions. In this work, the conversion characteristics of coal char in CLOU conditions were investigated for the first time.

Since the conversion rate of solid fuels is significantly promoted in CLOU in comparison to that in *i*G-CLC [5,6], many CLOU researchers only paid attention to the contribution of the oxidation reaction, while ignoring the contribution of gasification reaction which is actually the dominant reaction in *i*G-CLC. Recently, in our batch fluidized bed experiments, when the fluidizing agent in the reduction stage of CLOU was switched from N_2 to CO_2, a detectable increase of the instantaneous carbon conversion rate was observed [7]. In this sense, we deduced that the contribution of gasification in a real CLOU process was underestimated. As the first and necessary step, the char conversion characteristics in rich-CO_2 and lean-O_2 environment without the presence of OC and H_2O were investigated in this work prior to further revealing the complicated competitive reactions involved in CLOU processes.

Basically, the effects of CO_2 on char combustion/gasification have been extensively studied in both air-fired and oxy-fired processes. In air-fired processes [8–12], the CO_2 concentration around char particles is relatively low, which is quite different from that in oxy-fuel combustion. Chen et al. [13] summarized the effect of a CO_2-rich environment on the combustion rate of coal char. As shown in Fig. 2, three regions of char conversion in CO_2-rich conditions were distinguished according to the reaction temperature and O_2 concentration. The region A represents the low temperature conditions at any O_2 concentration. In this region, the CO_2-rich atmosphere has negligible effect on the char conversion rate. This is because, on one hand, the activity of CO_2 towards coal char is much lower than that of O_2 at relatively low temperatures, and CO_2 barely affects the oxidation process from the perspective of reaction mechanism; on the other hand, the oxidation of coal char is not strongly limited by the gas diffusion, thus the influence of O_2 diffusivity in different carrier gases (N_2 or CO_2) on the overall char conversion rate is not significant. The region B represents the high temperature and high O_2 concentration conditions, which are also the typical oxy-fuel combustion conditions. In this region, the oxidation reaction of coal char is easily controlled by the external diffusion (zone III), so the lower O_2 diffusivity in CO_2 than that in N_2 will significantly affect the oxidation reaction, and this effect becomes the dominant influencing factor on the oxidation consumption rate of coal char. The region C corresponds to the reaction conditions with high temperature and low O_2 concentration. In this region, on the one hand, the oxidation consumption rate of coal char is relatively low due to the low O_2 concentration; on the other hand, the gasification consumption rate of coal char increases significantly at high temperatures due to the higher activation energy of the gasification reaction. The presence of CO_2 can promote the conversion rate of coal char, because the improved gasification consumption rate exceeds the decrease of the oxidation consumption rate caused by the lowered O_2 diffusivity. However, Chen et al. [13] also pointed out that the above conclusions were attained from simplified models, in which the interactions of the heterogeneous and homogeneous reactions, the multi-component diffusion within and around the porous char particle, and the decrease of particle temperature due to the endothermic gasification reaction, had not been carefully considered. Therefore, more comprehensive simulations are still required for a better understanding.

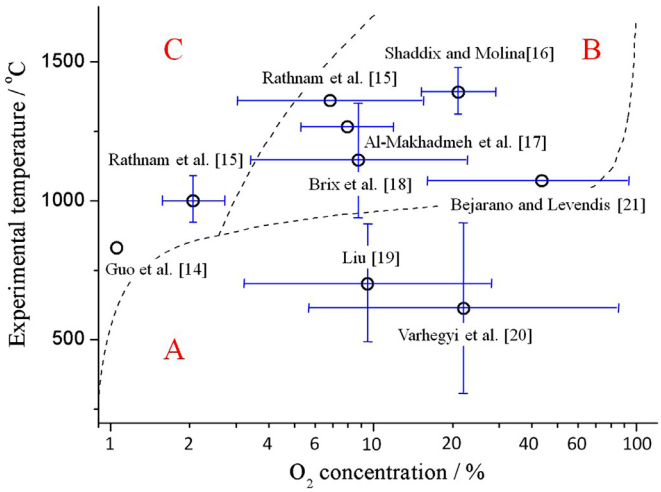

Fig. 2. Experimental studies on CO_2 effect in oxy-fuel conditions [13–21].

Gonzalo-Titado et al. [22] adopted the single-film model coupled with entrained flow reactor (EFR) experiments to investigate the impact of CO_2-gasification reaction for three coals with different ranks under oxy-fuel conditions, with the reaction temperatures of 1073–1723 K and O_2 concentrations of 4–8 vol.%. They concluded that the contribution of CO_2 gasification in O_2/CO_2 condition cannot be simply ignored, especially in the cases of low rank coal and lean-O_2/rich-CO_2 conditions. Brix et al. [23] simulated the conversion process of coal char particles in O_2/N_2 and O_2/CO_2 atmosphere by the established COCOMO (Coal Combustion MOdel) model. Experiments were also carried out in an EFR within the temperature range of 1173–1673 K and O_2 molar fraction range of 5–28 vol.%. Experimental results indicated that the CO_2 gasification has no effect on coal char conversion, while simulation results demonstrated that in zone III, the contribution of gasification can reach 70% when the O_2 concentration is low. In fact, although the COCOMO model considered both the internal and external diffusion effects, this model was still based on a simplified correlation at a macroscopic level (*e.g.* the effectiveness factor-Thiele modulus correlation), and only two global reactions were considered for the oxidation and gasification reactions. Therefore, the simulation results based on the COCOMO model might be qualitatively correct but not quantitatively accurate enough. Tolvanen et al. [24] developed a single particle model, which considered the heat transfer in the porous particle, the gas diffusion in the boundary layer and

Stefan flow. Particle size distribution was seriously treated in this model. Drop tube reactor (DTR) experiments (1123 K, 2–8 vol.% of O_2) were carried out for comparison with the simulations. They concluded that the polydispersity of char particles should be carefully considered in order to explain the wide distribution of the particle surface temperatures detected in experiments. Moreover, with the increase of CO_2 concentration, the decrease of particle surface temperature due to the endothermic gasification reaction becomes more remarkable, yet no obvious interaction or competition between gasification reaction and oxidation reaction was observed. Hecht et al. [25] simulated the combustion of coal char under oxy-fuel condition using the Surface Kinetics in Porous Particle (SKIPPY) code, with O_2 concentrations in the range of 12–36 vol.% and at 1690 K. The influence of CO_2 and H_2O on the conversion of the coal char particle was investigated in details. Besides heat transfer in the porous particle and gas diffusion in the boundary layer, the multi-component diffusion in the porous particle and the detailed homogeneous and heterogeneous reaction kinetics were also considered in the SKIPPY code. They found that the gasification reaction will decrease the temperature of burning particles, but the contribution of gasification consumption exceeds the decrease of oxidation consumption caused by the decreased particle temperature. Eventually, rich CO_2 promotes the overall conversion rate of coal char. Singer et al. [26] pointed out that because of the influence of volatile flame, the high temperature and high oxygen concentration conditions studied by Hecht et al. [25] in their steady-state single particle simulation may unrealistic in the oxy-fuel combustion. Through CFD simulation, they chose two representative particle trajectories, and divided them into three regions, respectively, *i.e.*, pre-flame, flame and post-flame. Using a more elaborate model, the single particle simulations with transient boundary conditions were then carried out to model the conversion process of coal char particle in a real oxy-combustion environment. They concluded that gasification contributes little to the consumption of coal char particles in path 1 (along the edge of the flame) where the temperature is not too high and the O_2 concentration is not too low. In path 2 (along the flame axis), the gasification contributes 2–3 times higher than the oxidation to char particle consumption, because the temperature in the flame region is very high and the concentration of oxygen is nearly close to 0. In post-flame region, the increased oxygen concentration and the decreased temperature lead to the decrease of the gasification contribution, but it still accounts for 13.8%–28.6% of the total char consumption rate. Generally, the contribution of the gasification conversion cannot be neglected under the oxy-combustion condition, and it should be carefully analyzed according to the specific reaction conditions of the char particle.

Particle-resolved simulation (*e.g.* the SKIPPY model) which considers the heat and mass transfer inside and outside the porous particle as well as the detailed chemical reaction kinetics is a very powerful tool to study the coal char conversion characteristics. Mitchell et al. [27] carried out a particle-resolved simulation to study the burning behavior of a coal char particle in zone I and zone II. Through the simulation, it was confirmed that the correlation of the Thiele modulus with the effectiveness factor for the first-order oxidation reaction is still valid in zone II. The potential relationship between the burning mode parameter and the effectiveness factor was also revealed. Nowadays, the conclusion that the burning mode parameter is equal to the effectiveness factor has been widely used by many researchers in their macroscopic level simulation [28,29]. The work of Mitchell et al. [27] provided a good example to construct macroscopic scale model from mesoscopic/microscopic scale simulations.

By far, although the influence of CO_2 on the oxidation process of coal char has been qualitatively investigated (to identify whether CO_2 affects the oxidation process and how it affects), the quantitative relationship of the coal char conversion rate in the mixed O_2/CO_2 atmosphere as a function of lean-O_2 oxidation rate and rich-CO_2 gasification rate has rarely been explored. In region B (as shown in Fig. 2), the O_2 diffusivity is the dominant influencing factor, and this effect can still be quantitatively considered in the corresponding combustion model (*e.g.* the single-film model [30]). However, in region C (typical CLOU operating conditions belong to this region), the contribution of the gasification could be significant, but quantitative contribution of the gasification and the intrinsic physicochemical mechanisms are still not clear, let alone developing a convincing macroscopic model for the char conversion rate. This brings huge difficulties to the simulation of char conversion process at the macroscopic level (*i.e.* CFD simulation). In this work, a particle-resolved model, which considered the heat and mass transfer inside and outside the porous particles as well as the detailed reaction kinetics, was established to simulate the conversion process of a coal char particle in typical CLOU conditions (with high concentration of CO_2 and low concentration of O_2). The interactions between the oxidation reaction and gasification reaction were analyzed, and a model to calculate the overall conversion rate of coal char in CLOU conditions was proposed.

2. Model description

For gas phase, the species mass conservation equation and energy conservation equation were established as below.

2.1. Species mass conservation equation

$$\frac{\partial}{\partial t}(\rho\phi Y_k)+\frac{1}{A}\frac{\partial}{\partial r}(\rho V_k A Y_k)=\dot{s}_k W_k \sigma_r+\dot{\varpi}_k W_k \phi \tag{1}$$

where, r is the radial spatial coordinate (m); ρ expresses the gas density (kg/m^3); $A=4\pi r^2$, is the area normal to the direction of r (m^2); ϕ express the porosity of the particle; Y_k represents the mass fraction of the kth species; V_k is the diffusion velocity of the kth species (m/s), and its calculation method will be described in Section 2.5.2; $\dot{s}_k$ is the molar rate of the production of the kth species per unit area by surface reactions (mol/(m^{2}s)); W_k is the molar weight of the kth species (kg/mol); and σ_r is the specific surface area per unit space volume (m^2/m^3). $\dot{\varpi}_k$ is the molar rate of production of the kth species per unit volume by gas-phase reactions (mol/m^{3}s).

2.2. Energy conservation equation

$$\frac{\partial}{\partial t}(\rho\phi\bar{h}+\rho_{tr}(1-\phi)h_p)+\frac{1}{A}\frac{\partial}{\partial r}\sum_{k=1}^{K_g}(\rho V_k A Y_k h_k)+\frac{1}{A}\frac{\partial}{\partial r}\left(-\lambda_t A\frac{dT}{dr}\right)$$
$$=-\sum_{k=1}^{K_g}\dot{\varpi}_k W_k \phi h_k-\sum_{k=1}^{K_{tot}}\dot{s}_k W_k \sigma_k h_k-\left.\frac{\varepsilon\sigma(T^4-T_W^4)}{\Delta r}\right|_{surf} \tag{2}$$

where, $\bar{h}$ and h_k represent the specific enthalpy of the gas mixture and the kth species, respectively (J/kg); ρ_{tr} is the true density of the char particle (kg/m^3); h_p is the specific enthalpy of the solid phase (J/kg); K_g is the total number of gas species; T is the reaction temperature (K); It was assumed that the solid phase and the gas phase are always in thermal equilibrium in this work, thus the temperatures of the solid phase and gas phase are both equal to the specified T; $\lambda_t=\lambda\phi+\lambda_p(1-\phi)$, the total thermal conductivity (W/(mK)); λ, the mixture-averaged gas thermal conductivity (W/(mK)); λ_p, the thermal conductivity of the solid particle (W/(mK)); K_{tot} is the total number of the species, including the gas, surface and bulk species; the last term in the formula is the

radiation source term, which should be included only for the outermost grid; T_W represents the equivalent wall temperature (K); ε and σ represent the emissivity and the Stefan-Boltzmann constant, respectively; Δr is the thickness of the concentric annular volume elements (m); the radiation source term was not considered in this work, because the particle in fluidized bed reactor (commonly adopted in CLOU) is almost entirely obscured by other particles with almost the same temperature.

For solid phase, the surface site species conservation equation and the consumption rate equation were considered.

2.3. Surface site species conservation equation

$$\frac{dZ_k}{dt} = \frac{\dot{s}_k o_k}{\Gamma} - Z_k \frac{S_0^2}{S}\left(\frac{S^2}{S_0^2} - \frac{\psi}{2}\right)\dot{s}_{C(B)} W_C \tag{3}$$

where, Z_k is the site fraction of the surface species k; o_k is the number of sites that species k occupies; Γ represents the density of site (mol/m^2); $\dot{s}_{C(B)}$ is the molar rate of the production of C(B) per unit area by surface reactions (mol/(m^{2}s)); W_C is the molar weight of the carbonaceous material; the specific surface area, S, (its initial value, S_0) and the structural parameter, ψ, will be described in Section 2.5.3. The dynamic surface assumption studied in Campbell [31] was used here.

2.4. Consumption rate equation of solid phase

$$\frac{d\rho_{ap}}{dt} = \dot{s}_{C(B)} \sigma_r W_C \tag{4}$$

where, ρ_{ap} is the apparent density of the char particle (kg/m^3).

Other important expressions related to the thermal and transport properties of gas phase, the morphological properties of the solid phase were described as follows.

2.5. Important relational expressions

2.5.1. Equation of state of the ideal gas

$$\rho = \frac{p\bar{W}}{RT} \tag{5}$$

where, p is the pressure (Pa); $\bar{W}$ is the mean molecular weight (kg/mol); R represents the universal gas constant (J/(mol K)).

2.5.2. Diffusion velocity

In this work, the mixture-averaged method in CHEMKIN [32] was used to calculate the transport properties, as:

$$V_k = V_{1k} + V_{2k} + V_{3k} \tag{6}$$

where, $V_{1k} = D_{km}\frac{1}{X_k}\frac{dX_k}{dr}$, is the ordinary diffusion velocity; $D_{km} = \frac{1-Y_k}{\sum_{j\neq k}^{K_g} X_j/D_{kj}}$, is the mixture-averaged diffusion coefficient; X_k represents the mole fraction of species k; D_{kj} is the binary diffusion coefficient; $V_{2k} = \frac{D_{km}\Theta_k}{X_k}\frac{1}{T}\frac{dT}{dr}$, is the thermal diffusion velocity, which was only considered for the low molecular weight species; Θ_k is the thermal diffusion ratio; the correction velocity V_{3k} was included to ensure that the mass fractions sum to unity or equivalently, $\sum_{k=1}^{K_g} Y_k V_k = 0$.

The diffusion velocity described above was only applied to the domain outside the porous particle. When it was used to the domain inside of the particle, the diffusion coefficient, D_{km}, should be adjusted and be replaced by the overall effective diffusion coefficient, D_{eff}, as:

$$\frac{1}{D_{eff}} = \frac{1}{D_{km,eff}} + \frac{1}{D_{K,k,eff}} \tag{7}$$

where, $D_{K,k,\,eff}$ is the effective Knudsen diffusion coefficient and is usually expressed as $D_{K,k,eff} = \frac{\phi}{\tau} D_{K,k}$; τ is the tortuosity of the particle; $D_{K,k} = \frac{2r_{pore}}{3}\sqrt{\frac{8RT}{\pi W_k}}$, the Knudsen diffusion coefficient; r_{pore} is the average pore radius (m); $D_{km,eff} = \frac{\phi}{\tau} D_{km}$, the effective bulk diffusion coefficient.

2.5.3. Correlations of the morphology parameters

The mean pore radius was based on the specific surface area (S, m^2/kg) and the pore volume per kilogram (ϕ/ρ_{ap}, m^3/kg) and was approximated using the following expression:

$$r_{pore} = \frac{2rf\phi}{\rho_{ap} S} \tag{8}$$

where, rf is a coefficient about the effects of wall roughness, and a value of 2 was applied in this work [27]. The porosity of the char particle can be calculated by the apparent density and the true density of the particle, as:

$$\phi = 1 - \frac{\rho_{ap}}{\rho_{tr}} \tag{9}$$

The local conversion and local specific surface area of the carbonaceous material were determined from the following relations:

$$x_C = 1 - \frac{\rho_{ap}}{\rho_{ap,0}} \tag{10}$$

$$\sigma_r = \sigma_{r,0}(1 - x_C)\sqrt{1 - \psi \ln(1 - x_C)} \tag{11}$$

$$S = \frac{\sigma_r}{\rho_{ap}} \tag{12}$$

where, x_C is the local conversion; $\rho_{ap,\,0}$ is the initial apparent density of the char particle (kg/m^3); $\sigma_{r,\,0}$ is the initial specific surface area per unit space volume (m^2/m^3). Obviously, it was assumed that the change of specific surface area follows the random pore model (RPM) [33], and the parameter, ψ, in this model is related to the pore structure. As shown in Singer and Ghoniem [34], the adaptive random pore model (ARPM) can be used to describe the pore structure evolution more accurately in the particle-resolved simulation. However, the two most important sub-models in modeling coal char particle conversion process are the pore structure evolution model and chemical kinetics model; note that the two sub-models are not independent. Once the ARPM model was adopted, the corresponding intrinsic elementary surface reaction kinetics should also be adopted. However, to the best of our knowledge, all available intrinsic elementary surface reaction kinetics of char in literatures was obtained based on the RPM model. And the transformation of the detailed reaction kinetics from RPM to ARPM is risky. In order to balance the credible description to the pore structure evolution and the appropriate representation to the chemical kinetics, the more mature model framework based on the random pore model and available intrinsic reaction kinetics was used in this work.

3. Simulation details

3.1. Mesh, initial and boundary conditions

Discretization of the above equations was based on the finite volume method. As shown in Fig. 3, the simulated particle was evenly divided into 100 concentric annular volume elements. The

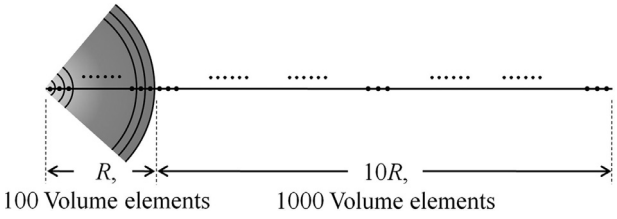

Fig. 3. Schematic view of the simulated particle and computational domain.

computational domain also included the spherical space within 10 times of the particle radius. In this case, the outermost element could be considered as in the ambient atmosphere, thus the boundary conditions for Eqs. (1) and (2) in the outer layer of char particle were set in accordance with the composition and temperature of the ambient gas. While the boundary conditions for Eqs. (1) and (2) at the char center were set to be zero gradient conditions, *i.e.*, $\frac{\partial Y_k}{\partial r} = 0$ and $\frac{\partial T}{\partial r} = 0$. At the beginning of the simulation, the whole computational domain was filled with N_2, the temperatures of all elements were equal to that of the ambient gas, and the surface active sites were all occupied by C(S), *i.e.* $Z_{C(S)} = 1$.

3.2. Computational strategy

The flowchart of the detailed algorithm is shown in Fig. 4. This algorithm was implemented as an application of the software CHEMKIN [32] in C language. The iterative solving steps were described as follows:

(1) Initialize all parameters, and set $t = 0$.
(2) Solve the energy, species and surface site equations in the inner loop until a convergence is realized.
(3) Let $t = t+\Delta t$, and continue.
(4) If the "Mix" sub-condition is being simulated, Eq. (4) will be solved and a new value of ρ_{ap} will be updated. The new ρ_{ap} at time t will be stored in the shared memory, and eventually be received by the "Oxid" and "Gasi" sub-condition simulations. In such a way, synchronization of the three sub-condition simulations was ensured.
(5) Update the other morphology parameters.
(6) If the local conversion, x_C, in the (solid particle) outermost grid is larger than 99.5%, the grid will be changed to a fluid grid.
(7) Calculate and output the interested parameters.
(8) If the overall conversion of the carbon particle is less than 99%, go to step (2).

As the data transmission and synchronization mechanisms described in Step 4 were used in the simulation, the evolutions of the morphology of the particles under both oxidation and gasification sub-conditions were ensured to be the same as that under the mixed O_2/CO_2 condition. Therefore, the three conversion rate curves which correspond to the three sub-conditions are ready for comparison with the same baseline. In other words, if the three coal char particles under the three sub-conditions are at the same overall conversion, they will have the same particle size, apparent density and specific surface area. This is also a requirement to develop an applicable macroscopic model, because in actual CLOU process, the morphology of coal char particle always evolves under the mixed O_2/CO_2 conditions, and the calculated oxidation and gasification rates (in order to calculate the overall conversion rate under the CLOU condition) are both based on the coal char particle whose morphology evolves under the mixed conditions.

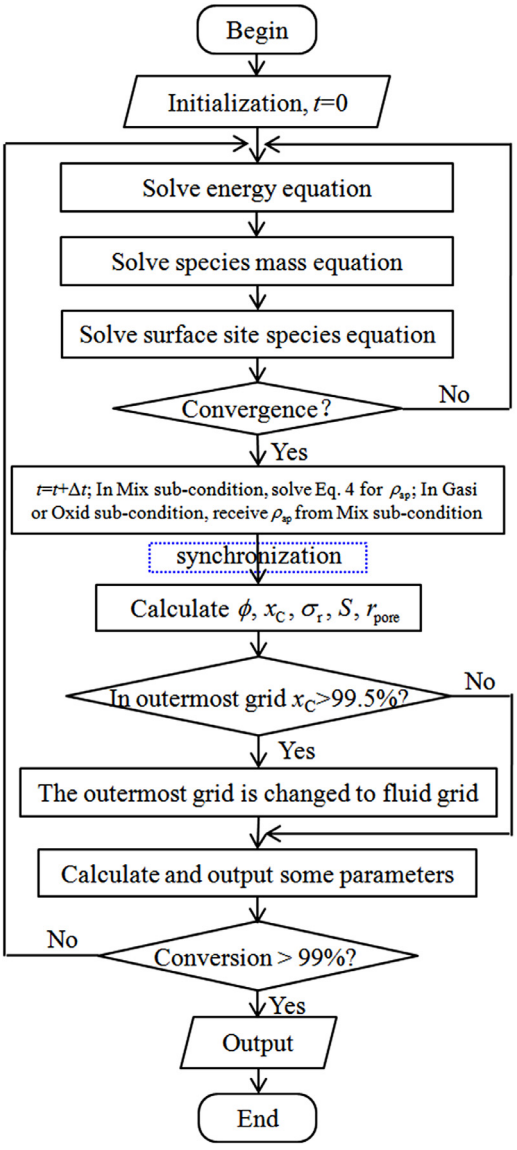

Fig. 4. Flowchart of the detailed algorithm.

3.3. Reaction kinetics and other parameters

Detailed heterogeneous reaction kinetics is indispensable in the particle-resolved simulations. Tilghman and Mitchell [35] have proposed a relatively complete surface reaction kinetics model for oxidation and gasification of coal char by summarizing former kinetics model and fitting experimental results conducted at relatively low temperatures. The detailed heterogeneous reaction kinetics rather than the Langmuir-Hinshelwood (L-H) type kinetics was used here to describe the competitive process of surface reactions, because the detailed reaction kinetics is more accurate for the description of the competitive process. Factually, the reaction kinetics in L-H form is one type of the global reaction kinetics, and it can be derived from the detailed elementary surface reaction kinetics, but is subject to the near-equilibrium or quasi-steady state hypotheses. However, these hypotheses cannot always be satisfied in reality (*e.g.* in the oxidation process). In the work of Mitchell et al. [27], the effect of homogeneous reactions was not considered, while in the work of Hecht et al. [25], the GRI-Mech 3.0 mechanism [36] was adopted to consider the effect of homogeneous reactions. The different considerations were

Table 1
Homogeneous reaction kinetics [36].

Reaction		A_i	B	E_i (cal/mol)
(Rg1)	2O+M↔O_2+M CO/ 1.75/ CO_2/ 3.60/	1.2×10^{17}	−1.0	0.0
(Rg2)	O+CO(+M)↔CO_2(+M) LOW/ 6.020×10^{14} 0.000 3000.00/ O_2/ 6.00/ CO/ 1.50/ CO_2/ 3.50/	1.8×10^{10}	0.0	2385.0
(Rg3)	O_2+CO↔O+CO_2	2.5×10^{12}	0.0	47,800.0

Table 2
Heterogeneous reaction kinetics of Wyodak coal char [35].

Reaction		A_i	E_i (cal/mol)
(Rs1)	C(O)+*C*(B)→CO+*C*(S)	1.55×10^{10}	59,629.54
(Rs2)	CO_2+*C*(S)↔C(O)+CO	3.70×10^{9}	38,479.92
(Rs3)	C(B)+2C(S)+O_2→C(O)+CO+*C*(S)	5.00×10^{20}	35,850.86
(Rs4)	2C(S)+O_2→C2(O2)	4.00×10^{17}	22,227.53
(Rs5)	C(S)+*C*(B)+*C*(O)+O_2→CO_2+*C*(O)+*C*(S)	1.50×10^{17}	18,642.45
(Rs6)	C(S)+*C*(B)+*C*(O)+O_2→CO+2C(O)	2.10×10^{17}	24,617.59
(Rs7)	C(B)+C2(O2)→CO_2+2C(S)	1.26×10^{9}	38,293.50

*The original parameters have been converted according to the standard format of CHEMKIN input.

Table 3
Other parameters used in the simulation [35].

Parameter	Unit	Value
Γ	(mol/m^2)	1.08×10^{-4}
$\sigma_{r,0}$	(m^2/m^3)	2.66×10^{8}
τ	(-)	3.0
ψ	(-)	8.0
Δt	(s)	1.0×10^{-5}
λ_p	(W/(mK))	1.33
ρ_{tr}	(kg/m^3)	1302
$\rho_{ap,0}$	(kg/m^3)	560

Table 4
Simulation conditions in the present work.

Run	Temperature of ambient gas / K	Particle diameter / μm	Molar fraction O_2 in oxidation sub-condition
1	1173	100	0.5%
2	1173	100	1.0%
3	1173	300	0.5%
4	1173	300	1.0%
5	1223	100	0.5%
6	1223	100	1.0%
7	1223	300	0.5%
8	1223	300	1.0%

probably due to the different temperature conditions that they simulated.

In this work, five species, O, O_2, CO, N_2 and CO_2, were considered in the gas phase, and any species containing element H were excluded, as the char was considered as an ash-free carbon particle. The three elementary reactions shown in Table 1 were obtained by eliminating all elementary reactions containing H in the GRI-Mech 3.0 [36] mechanism and were gathered as the homogeneous reaction kinetics in the present simulation.

Three surface species, C(O), C2(O2), and C(S), as well as one bulk species, C(B), were considered in the heterogeneous reaction mechanism. The reaction kinetics for oxidation and gasification of Wyodak coal char proposed by Tilghman and Mitchell [35] was adopted in this work, as shown in Table 2.

The other parameters that used in the simulation were summarized in Table 3.

The simulation conditions were listed in Table 4.

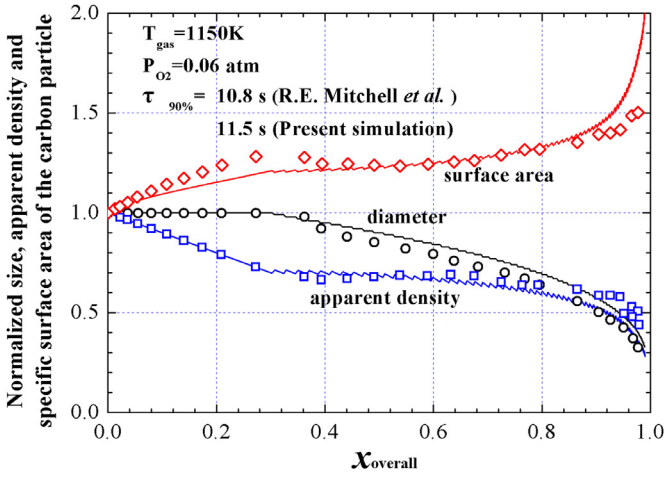

Fig. 5. Normalized size, apparent density and specific surface area *vs.* overall conversion of coal char particle: (dot) simulation results of Mitchell et al. [27], (line) simulation results of the present work.

4. Model validation

4.1. Validating the model and simulation program

In order to validate the model and simulation program, a case within the weak zone II burning region (see Mitchell et al. [27]) was simulated. The program used for this validation was obtained after a slight change to Step 4 of the above program (using the "Mix" condition for simulation, while removing the synchronization). The kinetic parameters and other model parameters for this validation were summarized in Section S1 in Supplementary material. The simulation results were shown in Fig. 5. The time required for the char particle to reach 90% conversion ($\tau_{90\%}$) is 11.5 s in the present simulation, which is in good agreement with the result of 10.8 s in Mitchell et al. [27]. Meanwhile, the normalized particle size, apparent density and specific surface area *vs.* the overall char conversion also agree well with the reference results. The small differences may be mainly ascribed to different mesh structures and/or model details. For example, the lumped parameter method was used to describe the energy conservation, and the heat and mass transfer correlations was considered as boundary conditions in Mitchell et al. [27].

4.2. Validating the heterogeneous reaction kinetics

The desorption kinetics was described by the distributed activation energy method in the original surface reaction mechanism in Tilghman and Mitchell [35] and Mitchell et al. [27]. However, it is not applicable in the CHEMKIN [32] that we adopted. Therefore, we first conducted a fitting process to deal with these desorption kinetics. We calculated the reaction rates at different temperatures according to the distributed activation energy, and then determined the new activation energy and pre-exponential factor by Arrhenius fitting. It should be pointed out that the final Arrhenius fitting demonstrated good linearity as long as the standard deviation of the activation energy in the distributed activation energy description is not very large.

In order to validate the kinetic parameters, the evolutions of the normalized mass loss rate of a single reaction point (the simplification of a particle when it is not affected by internal diffusion) were simulated at different temperature and gaseous composition conditions (see Fig. 6), which were then compared with the results of Tilghman and Mitchell [35]. The simulation details and some model parameters for the simulation were

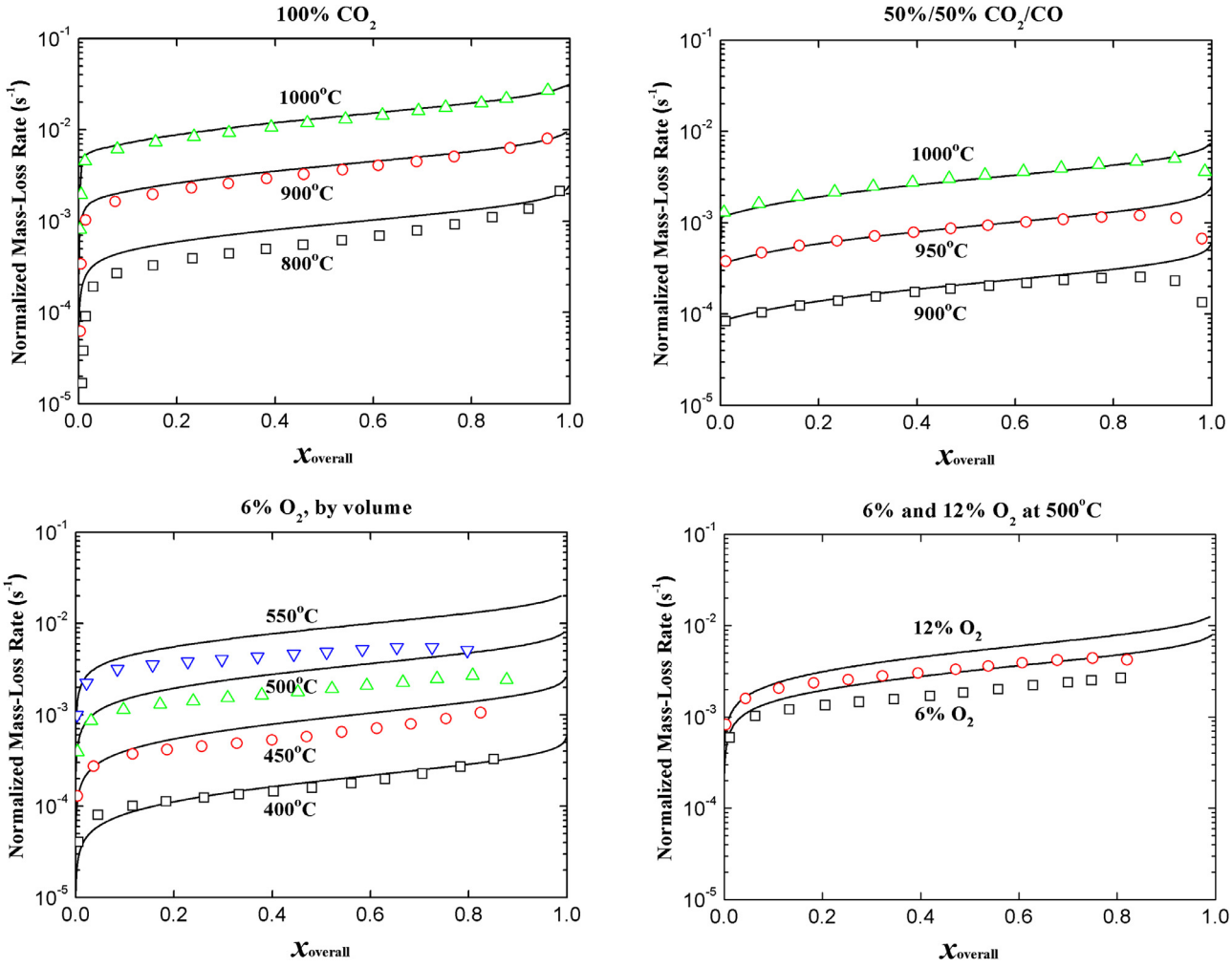

Fig. 6. Normalized mass loss rate *vs.* conversion at different temperature and gaseous composition conditions: (dot) simulation results in Tilghman and Mitchell [35], (line) simulation results in this work.

introduced in Section S2 in Supplementary material. Considering the difference of the mathematical model and numerical accuracy between the two simulations, it can be concluded that the two results were in good agreement with each other.

5. Results and analyses

Figure 7 shows the profile of the overall conversion rate of the simulated particle under the specified simulation conditions. As can be seen, the coal char conversion rate by oxidation reaction is higher than that by gasification reaction under CLOU conditions, and the conversion rate under the mixed sub-condition is higher than that under the oxidation sub-condition, but is lower than the sum of the conversion rate under the oxidation and gasification sub-conditions. Moreover, with the increase of the particle size, the contribution of gasification under the mixed sub-condition increases. The same tendency was also observed with the increase of temperature. The influence of the temperature is easy to understand: the activation energy of the global gasification reaction is greater than that of the global oxidation reaction. With the increase of temperature, the increase of the gasification reaction rate is larger than that of the oxidation reaction rate.

In typical CLOU conditions, the OC possesses a relatively low equilibrium O_2 partial pressure. Moreover, the actual O_2 concentration in FR may be even lower as the oxygen release process is usually the rate limiting step in the coal-derived CLOU process. Here, as a typical analytical condition, the conversion characteristics of a coal char particle with the diameter of 300 μm at 1223 K, under the reactive atmosphere of 0.5 vol.% O_2/N_2 (oxidation sub-condition), 99.5 vol.% CO_2/N_2 (gasification sub-condition) and 0.5 vol.% O_2/CO_2 (mixed sub-condition) were investigated in details.

Figure 8 shows the radial profile of the mole fractions of main gas components at 30.5 s (corresponding to 29.92% of the overall char conversion) under the typical analytical condition. It can be seen that the mole fractions of the main gas components do not change significantly from the bulk atmosphere ($r = 10R$) to the particle surface ($r = R$) under all the three sub-conditions, which indicated that the effect of the external diffusion is not significant and thus the high concentration of CO_2 do not affect the oxidation rate by inhibiting the O_2 diffusivity in these cases. Under the gasification sub-condition, the mole fraction of CO_2 decreases less than 8% from the particle surface ($r = R$) to the particle center, indicating that the internal diffusion has little effect on the overall conversion rate in the gasification sub-condition. However, under the oxidation and the mixed sub-conditions, the mole fraction of O_2 decreases rapidly at the external layer of the particle and almost approaches to 0 at $r/R = 0.8$. It is generally believed that the oxidation reaction of coal char at 1223 K belongs to the zone II burning region. The simulation results did show that the oxidation reaction is greatly affected by internal diffusion under such conditions. It is worth noting that the mole fraction of O_2 under the oxidation

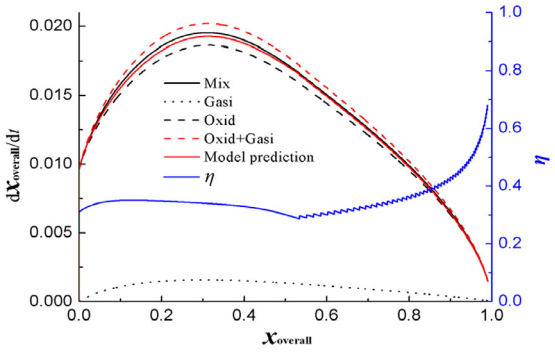

d_p=100μm, T_{bulk}=1173K, Oxid: 0.5 vol.% O_2/N_2, Gasi: 99.5 vol.% CO_2/N_2, Mix: 0.5 vol.% O_2/CO_2

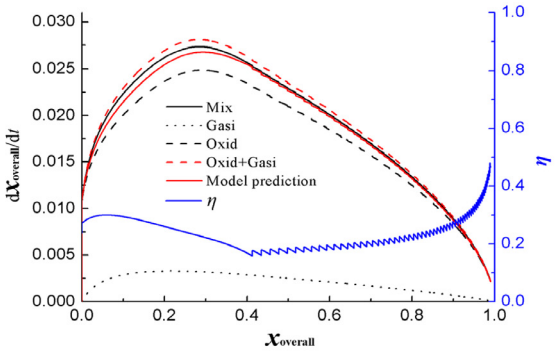

d_p=100μm, T_{bulk}=1223K, Oxid: 0.5 vol.% O_2/N_2, Gasi: 99.5 vol.% CO_2/N_2, Mix: 0.5 vol.% O_2/CO_2

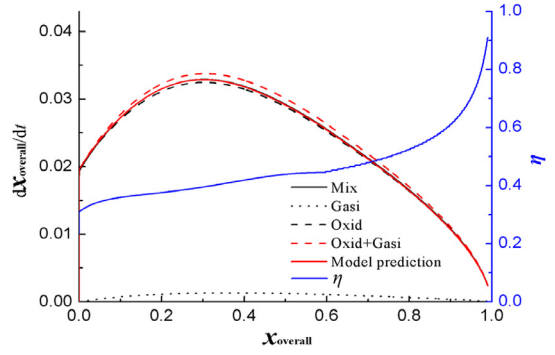

d_p=100μm, T_{bulk}=1173K, Oxid: 1 vol.% O_2/N_2, Gasi: 99 vol.% CO_2/N_2, Mix: 1 vol.% O_2/CO_2

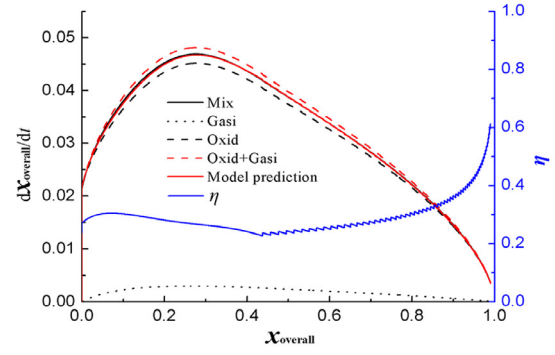

d_p=100μm, T_{bulk}=1223K, Oxid: 1 vol.% O_2/N_2, Gasi: 99 vol.% CO_2/N_2, Mix: 1 vol.% O_2/CO_2

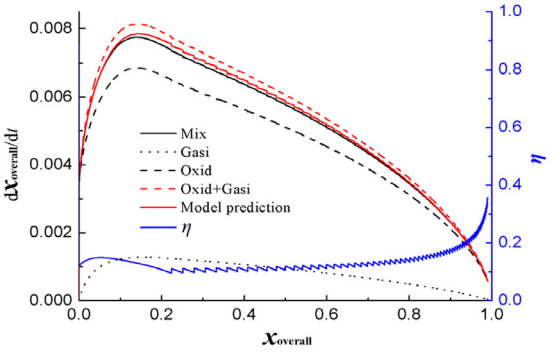

d_p=300μm, T_{bulk}=1173K, Oxid: 0.5 vol.% O_2/N_2, Gasi: 99.5 vol.% CO_2/N_2, Mix: 0.5 vol.% O_2/CO_2

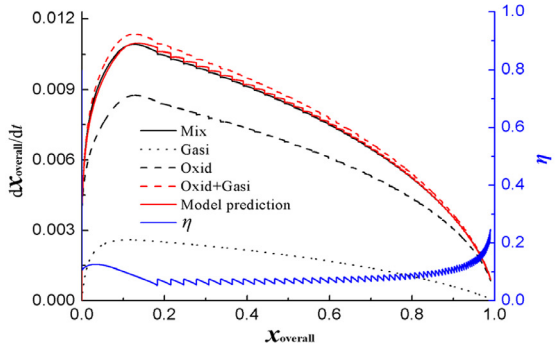

d_p=300μm, T_{bulk}=1223K, Oxid: 0.5 vol.% O_2/N_2, Gasi: 99.5 vol.% CO_2/N_2, Mix: 0.5 vol.% O_2/CO_2

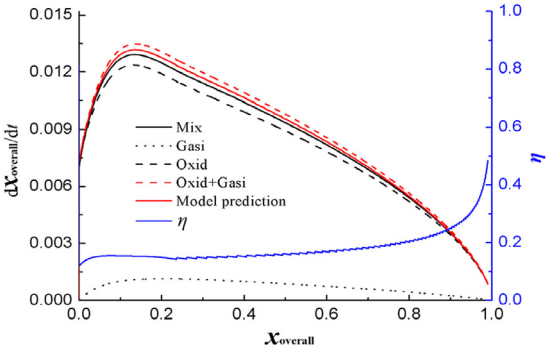

d_p=300μm, T_{bulk}=1173K, Oxid: 1 vol.% O_2/N_2, Gasi: 99 vol.% CO_2/N_2, Mix: 1 vol.% O_2/CO_2

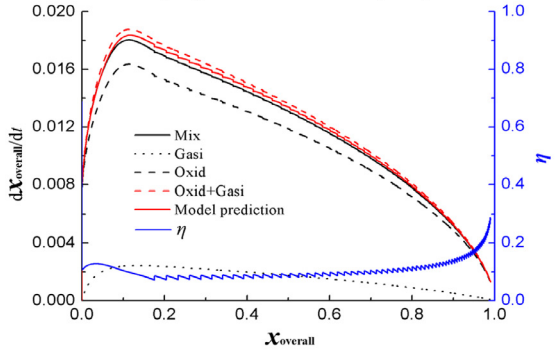

d_p=300μm, T_{bulk}=1223K, Oxid: 1 vol.% O_2/N_2, Gasi: 99 vol.% CO_2/N_2, Mix: 1 vol.% O_2/CO_2

Fig. 7. Overall conversion rates of the simulated char particles.

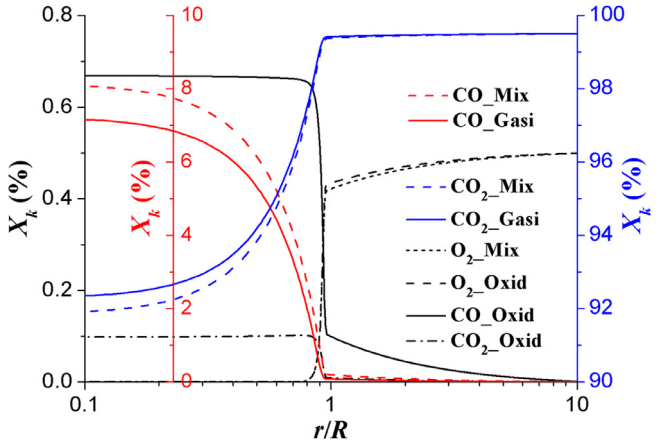

Fig. 8. Radial profile of the mole fractions of the main gas components at 30.5 s. (d_p = 300 μm, T_{bulk} = 1223 K, Oxid: 0.5 vol.% O_2/N_2, Gasi: 99.5 vol.% CO_2/N_2, Mix: 0.5 vol.% O_2/CO_2).

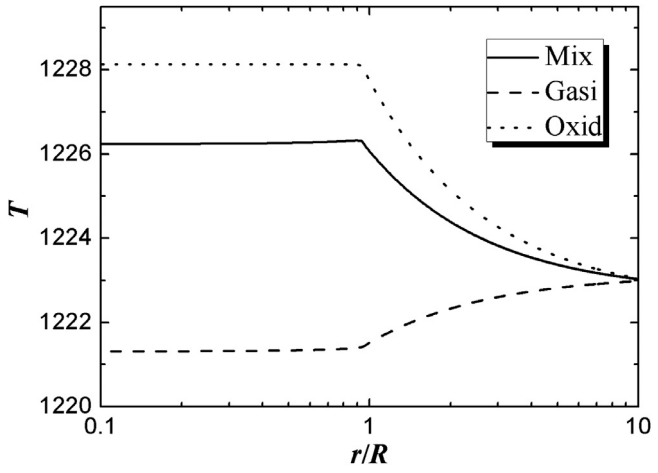

Fig. 9. Radial profile of the temperatures at 30.5 s. (d_p = 300 μm, T_{bulk} = 1223 K, Oxid: 0.5 vol.% O_2/N_2, Gasi: 99.5 vol.% CO_2/N_2, Mix: 0.5 vol.% O_2/CO_2).

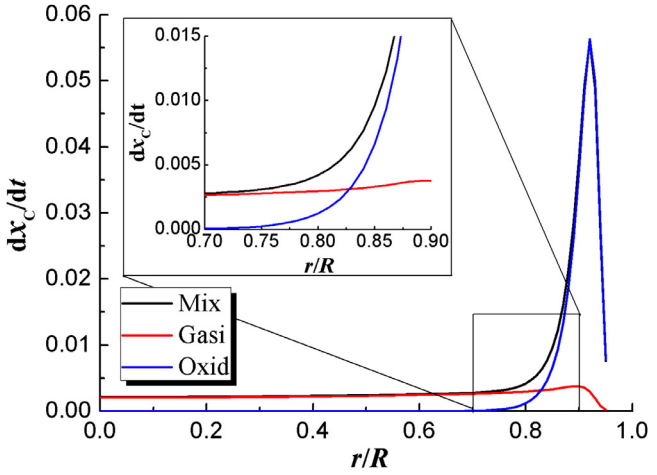

Fig. 10. Radial profile of the local conversion rates in three sub-conditions at 30.5 s. (d_p = 300 μm, T_{bulk} = 1223 K, Oxid: 0.5 vol.% O_2/N_2, Gasi: 99.5 vol.% CO_2/N_2, Mix: 0.5 vol.% O_2/CO_2).

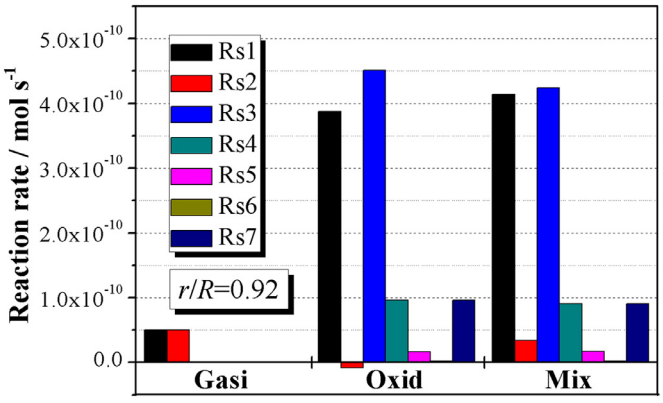

Fig. 11. Reaction rates of the elementary surface reactions at 30.5 s and r/R = 0.92. (d_p = 300 μm, T_{bulk} = 1223 K, Oxid: 0.5 vol.% O_2/N_2, Gasi: 99.5 vol.% CO_2/N_2, Mix: 0.5 vol.% O_2/CO_2).

sub-condition and mixed sub-condition shows almost the same evolution trend, which also suggests that CO_2 has little effect on the oxidation process.

The radial profile of the temperatures at 30.5 s under the typical analytical condition is shown in Fig. 9. Because of the endothermicity of the gasification reaction, the mean temperature of the char particle is 1.7 K lower than that of the ambient gas in the gasification sub-condition. The char oxidation reaction is exothermic, thus the mean temperature of the char particle is 5.1 K higher than that of the ambient gas in the oxidation sub-condition. In the mixed sub-condition, the endothermic gasification reaction reduces the char particle temperature from 1228.1 K to 1226.2 K. Nevertheless, all changes of the temperature from the heterogeneous reactions are not significant, thus it can be concluded that the high concentration of CO_2 in typical CLOU conditions hardly affects the oxidation rate through reducing the particle temperature.

The radial profile of the local conversion rates at 30.5 s under the typical analytical condition is shown in Fig. 10. Similar to the profile of O_2 concentration shown in Fig. 8, the char conversion rate reaches the maximum value at the external layer of the particle and generally decreases from the particle surface to the particle center under the oxidation and mixed sub-conditions. Moreover, the curve under the mixed sub-condition coincides almost with that under the oxidation sub-condition in the external layer of the particle, which suggests that in the mixed sub-condition, the char conversion in the external layer of the particle is mainly attributed to the oxidation reaction. In the interior of the particle, the char conversion rate approaches to zero under the oxidation sub-condition, but the curve of the conversion rate under the mixed sub-condition is close to that under the gasification sub-condition, indicating that the char mainly undergoes gasification in the interior of the particle. The char conversion rate increases from r/R = 0.95 to r/R = 0.9 both under the oxidation and mixed sub-conditions, which is because according to the random pore model, there is a maximum surface area at a medium value of the conversion. Factually, in the simulation, the local conversion in the external layer of the particle has been larger than this medium value, thus the smaller local conversion at r/R = 0.9 than that at r/R = 0.95 results in the larger local surface area and local conversion rate at r/R = 0.9 than those at r/R = 0.95.

The reaction rates of all elementary surface reactions at 30.5 s and the position of r/R = 0.92 under the typical analytical condition are shown in Fig. 11. It can be seen that the high concentration of CO_2 does affect the oxidation reaction, but this influence is not very significant. The influence is mainly manifested in these aspects: the negative reaction rate of Rs2 in the oxidation sub-condition changes to the positive reaction rate in the mixed sub-condition; the reaction rates of Rs1 and Rs3 become larger and smaller from the oxidation sub-condition to the mixed sub-condition, respectively. It is mainly because the concentration

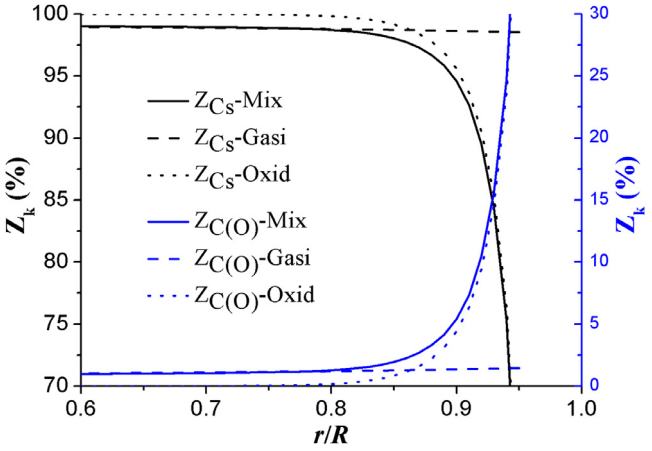

Fig. 12. Radial profile of the site fractions of the surface components at 30.5 s. (d_p = 300 μm, T_{bulk} = 1223 K, Oxid: 0.5 vol.% O_2/N_2, Gasi: 99.5 vol.% CO_2/N_2, Mix: 0.5 vol.% O_2/CO_2).

of CO_2 under the mixed sub-condition is far larger than that under the oxidation sub-condition. According to the surface reaction mechanism shown in Table 2, the presence of CO_2 can affect the equilibrium of Rs2 and further affect the site fractions of the surface species. More specifically, the high concentration of CO_2 leads to the shift of the equilibrium of Rs2 towards the right side, resulting in a decreased site fraction of C(S) and an increased site fraction of C(O).

Figure 12 shows the radial profile of the site fractions of the surface components at 30.5 s under the typical analytical condition. Two important points that support the above analyses can be attained: (1) in the external layer of the particle, the curve under the mixed sub-condition almost coincides with that under the oxidation sub-condition, while in the interior of the particle, it almost coincides with that under the gasification sub-condition; (2) at r/R = 0.92, the site fractions of C(S) and C(O) under the mixed sub-condition are smaller and larger than these under the oxidation sub-condition, respectively.

From the above analyses, it can be seen that the char conversion process under the mixed condition of lean O_2 and rich CO_2 can be regarded as a separate oxidation conversion process in the external layer of the particle and a gasification process in the interior of the particle. Although the high concentration of CO_2 has certain impact on the oxidation process, this influence is not very significant. Thus, the effect of rich CO_2 on the oxidation process can be ignored. As for the gasification process, the oxidation process exerts a little impact on the gasification process by changing the gasification atmosphere. The influence of the oxidation reaction on the gasification process is mainly reflected in that the predominant oxidation reaction happens in the external layer of the particle and inhibits the gasification reaction from the perspective of reaction mechanism. In such a way, it can be reasonably considered that the char gasification can only happen in the inner core of the particle rather than within the whole particle. Eventually, the phenomena shown in Fig. 7 can be reasonably explained. In fact, with the increase of the char particle size, the ratio of the gasification-controlled region to the oxidation-controlled region also increases.

Based on the above understandings, the macroscopic model for the char conversion rate in lean O_2 and rich CO_2 atmospheres can be represented as $r_{mix} = \varphi_1 \cdot r_{gasi} + r_{oxid}$, where r_{mix}, r_{gasi} and r_{oxid} are the char conversion rates in a specific particle state, *e.g.* particle radius, apparent density and specific surface area in the mixed sub-condition, the separated gasification condition, and the separated oxidation condition, respectively; φ_1 means the ratio of the conversion rate contributed by gasification under the mixed sub-condition to the conversion rate under the separated gasification condition. Clearly, φ_1 is related to the penetration depth of O_2, which can be characterized by the effectiveness factor of the oxidation reaction, η (can also be easily obtained in the macroscopic model, also presented in Fig. 7). Finally, the conversion rate of coal char particle under CLOU conditions can be modeled by

$$r_{mix} = \varphi_1(\eta) \cdot r_{gasi} + r_{oxid} \tag{13}$$

The macroscopic model for the char conversion rate can be illustrated by Fig. 13.

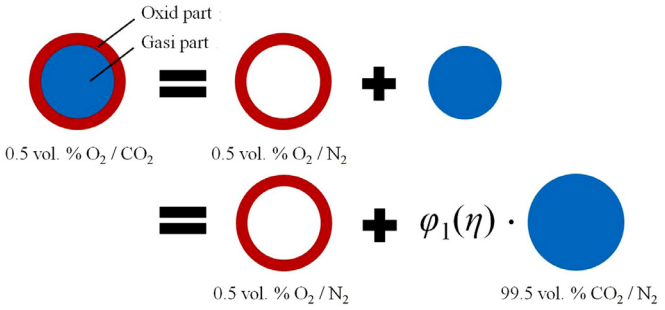

Fig. 13. Schematic view of the conversion of a coal char particle in CLOU conditions.

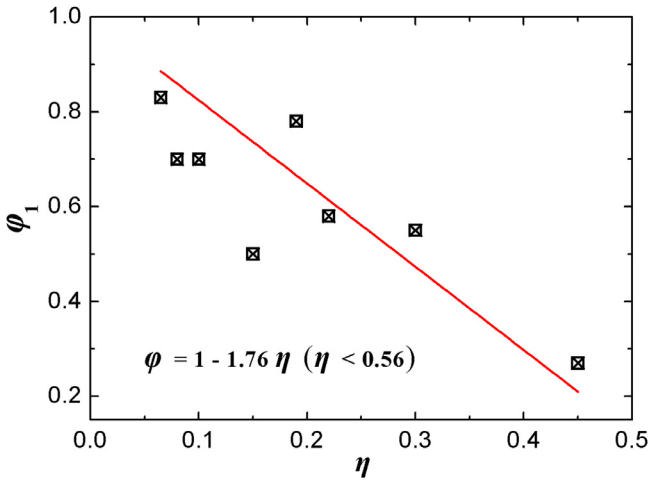

Fig. 14. Correlation between φ_1 and η.

According to the simulation results under CLOU conditions (as shown in Table 4), the correlation between φ_1 and η was fitted and plotted in Fig. 14.

Based on the fitting formula shown in Fig. 14 and the proposed macroscopic model (Eq. (13)), the conversion rates were calculated for each simulation condition and the results were also shown in Fig. 7. It can be seen that the proposed macroscopic model can well reproduce the particle-resolved simulation result of the char conversion rate in CLOU conditions.

6. Discussion

As mentioned in Introduction, the contribution of gasification on the overall conversion process of coal char depends on the reaction conditions, especially the reaction temperature and oxygen concentration. In this work, the simulation conditions were confined within the scope of CLOU. The conclusions attained in this work may only applicable for CLOU or similar conditions and cannot be arbitrarily applied to situations far away from these conditions, such as the oxy-combustion conditions. As concluded by Singer et al. [26], the gasification can contribute up to 30% of

overall conversion rate at 1573 K in the post-flame region of the oxy-fuel combustion.

Different coal chars have different reactivity, which is related to the complex porous structure in the mesoscopic level and the complex surface property in the microscopic level [37]. Although such difference may affect the oxidation and gasification rate as well as its relative contribution, the proposed methodology of integrating the oxidation and gasification conversion rate by considering the effectiveness factor of the oxidation reaction should still be applicable for different chars. This is because, as long as the oxidation reaction is still some orders of magnitude faster than that of the gasification reaction (typically, in CLOU conditions), the competing relationship between lean-O_2 oxidation and rich-CO_2 gasification still holds in nature.

H_2O was not considered in both homogeneous and heterogeneous reactions in this work, although H_2O is expected to be present via the conversion of H in coal or being introduced as fluidization and gasification agents in actual CLOU processes. The gasification rate of coal char by H_2O has long been believed to be 2–4 times faster than that of coal char gasification by CO_2. In this sense, it is reasonable to conjecture that the presence of H_2O may increase the contribution of gasification in the coal char conversion process. However, in comparison to the activity of coal char towards O_2, the intrinsic char-H_2O gasification process is still very slow, and it is also believed that the detailed surface reaction process of H_2O has little influence on the detailed surface reaction process of O_2. From this respect, the proposed methodology of integrating the oxidation and gasification conversion rate by considering the effectiveness factor of the oxidation reaction can still be applicable for the circumstances where H_2O is present; however, the specific quantitative relationship needs to be re-analyzed. With respect to the impact of H_2O on the homogeneous reactions, it has been well recognized that the presence of OH radical, one of the intermediate products in the presence of H_2O, will remarkably accelerate the conversion of CO in gas phase. However, because the overall char conversion rate is not very fast under the CLOU conditions, it seems that the concentration of CO (or H_2) in the boundary layer of the particle is not very high, thus the presence of H_2O may not have a significant impact on the gas phase reactions. Even so, the impact of H_2O deserves further investigation.

7. Conclusions

In this work, a single particle model, which considered the detailed reaction kinetics as well as the heat and mass transfer inside and outside the porous particles, was established for the subsequent particle-resolved numerical simulations, in order to investigate the contributions of the oxidation and gasification (only by CO_2) reaction to the overall char conversion, as well as their interactions under CLOU conditions. The main conclusions were drawn as follows:

(1) Unlike burning under the high temperature conditions, the oxidation process of coal char particle is almost not affected by external gas diffusion under typical CLOU conditions. Therefore, although the diffusivity of O_2 in CO_2 is lower than that in N_2, this effect was not important in modeling the overall char conversion rate under typical CLOU conditions. In addition, the influence of the endothermicity of the gasification reaction can also be ignored in typical CLOU conditions.

(2) The high concentration of CO_2 within the coal char particle and sequentially the rich CO_2-char gasification reaction hardly affects the oxidation process from the perspective of reaction mechanism.

(3) The influence of the oxidation reaction on the gasification process was mainly manifested in that the oxidation reaction happens in the external layer of the particle and inhibits the gasification reaction from the perspective of reaction mechanism. Therefore, the gasification reaction only happens in the inner core of the particle, rather than happens within the whole particle.

(4) As the penetration depth of O_2 can be reflected by the effectiveness factor of the oxidation reaction, η, the methodology of correlating φ_1 with η was proposed in this work, and the correlation was quantitatively determined by fitting the simulation results under typical CLOU conditions.

As only CO_2 gasification was considered in this work, the quantitative correlation determined may only applicable for the ideal condition of CLOU, *i.e.* there is no steam in the atmosphere. Because H_2O (as reaction product or gasification agent) is indeed present in a realistic CLOU process, further work will be undertaken to determine the role of steam within the char gasification process, including identifying the contribution of rich-CO_2/H_2O gasification on the char conversion and formulating the macroscopic model for the char conversion rate with the consideration of lean-O_2 oxidization and rich-CO_2/H_2O gasification.

Declaration of Competing Interest

The authors declare that they have no known competing financial interests or personal relationships that could have appeared to influence the work reported in this paper.

Acknowledgment

This work was supported by National Key R&D Program of China (2016YFB0600801).

Supplementary materials

Supplementary material associated with this article can be found, in the online version, at doi:10.1016/j.combustflame.2019.11.046.

References

[1] J. Adanez, A. Abad, F. Garcia-Labiano, P. Gayan, L.F.D. Diego, Progress in chemical-looping combustion and reforming technologies, Prog. Energ. Combust. 38 (2012) 215–282.
[2] J. Adanez, A. Abad, T. Mendiara, P. Gayan, L.F.D. Diego, F. Garcia-Labiano, Chemical looping combustion of solid fuels, Prog. Energ. Combust. 65 (2018) 6–66.
[3] L.S. Fan, F. Li, Chemical looping technology and its fossil energy conversion applications, Ind. Eng. Chem. Res. 49 (2010) 10200–10211.
[4] T. Mattisson, A. Lyngfelt, H. Leion, Chemical-looping with oxygen uncoupling for combustion of solid fuels, Int. J. Greenh. Gas Con. 3 (2009) 11–19.
[5] T. Mattisson, H. Leion, A. Lyngfelt, Chemical-looping with oxygen uncoupling using CuO/ZrO_2 with petroleum coke, Fuel 88 (2009) 683–690.
[6] E.M. Eyring, G. Konya, J.S. Lighty, A.H. Sahir, A.F. Sarofim, K. Whitty, Chemical looping with copper oxide as carrier and coal as fuel, Oil Gas Sci. Technol. 66 (2011) 209–221.
[7] K. Wang, H. Zhao, X. Tian, Y. Fang, J. Ma, C. Zheng, Chemical-looping with oxygen uncoupling of different coals using copper ore as an oxygen carrier, Energy Fuels 29 (2015) 6625–6635.
[8] D.J. Harris, I.W. Smith, Intrinsic reactivity of petroleum coke and brown coal char to carbon dioxide, steam and oxygen, Proc. Combust. Inst. 23 (1991) 1185–1190.
[9] A.P. Mann, J.H. Kent, A computational study of heterogeneous char reactions in a full-scale furnace, Combust. Flame 99 (1994) 147–156.
[10] B.R. Stanmore, S.P. Visona, The contribution to char burnout from gasification by H_2O and CO_2 during pulverized-coal flame combustion, Combust. Flame 113 (1998) 274–276.
[11] S. Kajitani, S. Hara, H. Matsuda, Gasification rate analysis of coal char with a pressurized drop tube furnace, Fuel 81 (2002) 539–546.
[12] R.E. Mitchell, O.H. Madsen, Experimentally determined overall burning rates of pulverized-coal chars in specified O_2 and CO_2 environments, Proc. Combust. Inst. 21 (1988) 173–181.

[13] L. Chen, S.Z. Yong, A.F. Ghoniem, Oxy-fuel combustion of pulverized coal: characterization, fundamentals, stabilization and CFD modeling, Prog. Energ. Combust. 38 (2012) 156–214.
[14] X. Guo, L.T. Hui, S. Zhang, C.Z. Li, Changes in char structure during the gasification of a Victorian brown coal in steam and oxygen at 800 °C, Energy Fuels 22 (2008) 4034–4038.
[15] R.K. Rathnam, L.K. Elliott, T.F. Wall, Y. Liu, B. Moghtaderi, Differences in reactivity of pulverized coal in air (O_2/N_2) and oxy-fuel (O_2/CO_2) conditions, Fuel Process. Technol. 90 (2009) 797–802.
[16] C.R. Shaddix, A. Molina, Effect of O_2 and high CO_2 concentrations on PC char burning rates during oxy-fuel combustion, 33rd international technical conference on coal utilization and fuel systems, Clearwater, FL, USA (2008).
[17] L. Al-Makhadmeh, J. Maier, G. Scheffknecht, Coal pyrolysis and char combustion under oxy-fuel conditions, 34th International Technical Conference on Coal Utilization Andfuel Systems, Clearwater, FL, USA (2009).
[18] J. Brix, P.A. Jensen, A.D. Jensen, Coal devolatilization and char conversion under suspension fired conditions in O_2/N_2 and O_2/CO_2 atmospheres, Fuel 89 (2010) 3373–3380.
[19] L. Hao, Combustion of coal chars in O_2/CO_2 and O_2/N_2 mixtures: a comparative study with non-isothermal thermogravimetric analyzer (TGA) tests, Energy Fuels 23 (2009) 4278–4285.
[20] G. Várhegyi, P. Szabó, E. Jakab, Mathematical modeling of char reactivity in Ar-O_2 and CO_2-O_2 mixtures, Energy Fuels 10 (1996) 1208–1214.
[21] P.A. Bejarano, Y.A. Levendis, Single-coal-particle combustion in O_2/N_2 and O_2/CO_2 environments, Combust. Flame 153 (2008).
[22] C. Gonzalo-Tirado, S. Jiménez, J. Ballester, Kinetics of CO_2 gasification for coals of different ranks under oxy-combustion conditions, Combust. Flame 160 (2013) 411–416.
[23] J. Brix, P.A. Jensen, A.D. Jensen, Modeling char conversion under suspension fired conditions in O_2/N_2 and O_2/CO_2 atmospheres, Fuel 90 (2011) 2224–2239.
[24] H. Tolvanen, R. Raiko, An experimental study and numerical modeling of combusting two coal chars in a drop-tube reactor: a comparison between N_2/O_2, CO_2/O_2 and $N_2/CO_2/O_2$ atmospheres, Fuel 124 (2014) 190–201.
[25] E.S. Hecht, C.R. Shaddix, M. Geier, A. Molina, B.S. Haynes, Effect of CO_2 and steam gasification reactions on the oxy-combustion of pulverized coal char, Combust. Flame 159 (2012) 3437–3447.
[26] S. Singer, L. Chen, A.F. Ghoniem, The influence of gasification reactions on char consumption under oxy-combustion conditions: effects of particle trajectory and conversion, Proc. Combust. Inst. 34 (2013) 3471–3478.
[27] R.E. Mitchell, L. Ma, B.J. Kim, On the burning behavior of pulverized coal chars, Combust. Flame 151 (2007) 426–436.
[28] N.E.L. Haugen, R.E. Mitchell, M.B. Tilghman, A comprehensive model for char particle conversion in environments containing O_2 and CO_2, Combust. Flame 162 (2014) 1455–1463.
[29] Z. Zhi, Z. Li, N. Cai, Reduced-order model of char burning for CFD modeling, Combust. Flame 165 (2016) 83–96.
[30] S. Li, Y. Xu, Q. Gao, Measurements and modelling of oxy-fuel coal combustion, Proc. Combust. Inst. 37 (2019) 2643–2661.
[31] P.A. Campbell, Investigation into the roles of surface oxide complexes and their distributions in the carbon-oxygen heterogeneous reaction mechanism, Stanford Univ, Palo Alto, California, USA, 2006.
[32] R.J. Kee, F.M. Rupley, J.A. Miller, M.E. Coltrin, J.F. Grcar, et al., CHEMKIN Release 4.1, R. Design (Ed.), (Ed.), San Diego, CA, 2006.
[33] S.K. Bhatia, D.D. Perlmutter, A random pore model for fluid-solid reactions: I. Isothermal, kinetic control, AIChE J 26 (1980) 379–386.
[34] S.L. Singer, A.F. Ghoniem, Comprehensive gasification modeling of char particles with multi-modal pore structures, Combust. Flame 160 (2013) 120–137.
[35] M.B. Tilghman, R.E. Mitchell, Coal and biomass char reactivities in gasification and combustion environments, Combust. Flame 162 (2015) 3220–3235.
[36] G.P. Smith, S.D. Golden, M. Frenklach, N.W. Moriarty, B. Eitener, M. Goldenberg, C.T. Bowman, R.K. Hanson, S. Song, W.C. Gardiner, V.V. Lissianski, Z. Qin, GRI-Mech 3.0, 2001. <http://www.me.berkeley.edu/gri_mech>.
[37] H. Zhao, X. Tian, J. Ma, M. Su, B. Wang, D. Mei, Development of tailor-made oxygen carriers and reactors for chemical looping processes at Huazhong University of Science & Technology, Int. J. Greenh. Gas Con. (2019) 102898, doi:10.1016/j.ijggc.2019.102898.